DOI: 10.21062/mft.2023.032 http://www.journalmt.com

Design of Dual-Head 3D Printer

Vlastimil Chalupa (0009-0003-6948-1535), Michal Stanek (0000-0001-8749-8996), Jiří Vanek (0009-0009-1692-1385), Jan Strnad (0009-0007-2830-534X), Martin Ovsik (0000-0002-1932-2814)
Faculty of Technology, Tomas Bata University in Zlin. Vavrečkova 5669, 760 01 Zlin, Czech Republic. Email: v_chalupa@utb.cz; stanek@utb.cz; j4_vanek@utb.cz; j2_strnad@utb.cz; ovsik@utb.cz

Fused Filament Fabrication (FFF) printers are usually designed to create a product with one single material. Some of them allow fabricating items in multiple colours but creating a single product consisting of two different materials remains an advantage of industrial 3D printers only. The aim of this research was to develop a design of a device with two printheads which enables to print products with two different materials, compatible with a cheap and commonly available FFF device Prusa i3MK2S, and the subsequent production of a prototype. A key aspect of the design was the hardware compatibility of the device with the given printer while maintaining the maximum possible printing area.

Keywords: dual extrusion, multi-material 3D print, FFF printer

1 Introduction

3D printing (extrusion) is a modern and quickly developing technology working on the principle of folding the material into layers. A big advantage lies in the use of these printers in the production of functional prototypes, models, pieces, or small series manufacturing. It is also possible to print whole assemblies and other complicated products. The most widespread type of 3D printing is the FFF (Fused Filament Fabrication) method, the use of which ranges from hobby printing, through the mechanical, aerospace, and automotive industries up to medical use.

Most machines using this technology only have one printhead (extrusion head) and can print the product from only one material. On the other hand, industrial 3D printers can usually use two printing heads, but the purchase price of such equipment is several orders of magnitude higher than in case of a conventional 3D printer. At present, several research papers focus on upgrades of 3D printers in different ways, e.g., changes of the motor specification, modification, or addition of printheads to enable printing products with two different materials or use soluble supports.

The benefits of printhead addition were discussed by Reiner et al. [17] and Ali et al. [1] who both focused on the minimization of colour switching delay by employing multiple nozzles. On the other hand, Han et. al. [9] tried to approach this issue by developing a colour mixing nozzle for the FFF printer, which enabled the printing of multi-colour material with only a single nozzle. Also, Chen et al. [4] in his work dealing with the design and analysis of a mixing nozzle.

While the researchers focused on the enhancement of already existing printers, Kun et al. [12] reconstructed a custom dual-head 3D printer, using reverse engineering and 3D scanning. Finally, Sitthi-Amon et al. [19] took a different approach, and on top of a high-resolution multi-material machine added an integrated 3D scanning module to enable a closed-feedback loop capable of minor corrections in the print process, thus minimizing the colour switching delay.

The issue of dual extrusion is not only solved in the FDM method but also in 3D bioprinting. One possible solution to this problem is described by De La Nava et al. [6] He designs a solution based on a conventional 3D printer where the standard print head is replaced by two injection extruders enabling a controlled method of applying hydrogel-cell ink. While a 3D bioprinter with single ink can be calibrated using standard procedures, with a multi-head printer, calibration is much more difficult. Sodupe-Ortega et al. [20] provides a solution to this problem in the complexity of the relationship between printing parameters and printing resolution. The connection of a conventional FDM printer with a bioprinter was reported by Koch et al. [11] The redesign of the commercial printer concept enabled the production of components that consist of both polymer and gel extruded by syringe-based microextrusion printhead.

The use of 3D printing in medicine is becoming more widespread, and the resulting demand for anatomically accurate models brings the need to print products that simulate the interweaving of soft and hard tissues. Jaksa et al. [10] describes a solution to this problem using an available conventional 3D printer. A similar use of a dual-head 3D printer is found in medicine by Liimatainen et al. [14] when printing models of a tumor-infected organ, where healthy and infected tissues are printed from different material. Another example is in the work of Otepbergen et al. [16] the use of multimaterial 3D printing in the

preparation of an ankle orthosis made of PLA material which is locally reinforced with Nylon.

The combination of several 3D printing technologies is one of the ways to produce multi-component products. Roach et al. [18] describes a hybrid device combining fused filament fabrication, inkjet, aerosol jetting, intense pulsed light sintering, direct ink writing and two robotic manipulators. It demonstrates its function in products in the field of electronics, robotics and medicine. A dual printhead combining a conventional FDM method together with an endless fiber application head is described in Block et al. [3] With this technology, an endless fiber is applied and then pressed into a part. The resulting product is thus strengthened thanks to the properties of this fiber. Another use of a multi-jet 3D printer layout is according to Laureto et al. [13] printing of composite parts reinforced with metal wire. According to the proposed arrangement of the printing device, it is possible to produce reinforced polymer parts that excel in higher strength but also in electrical conductivity.

The general issue of multimaterial 3D printing is described by Bandyopadhyay et al. [2], where it highlights new possibilities to produce composite products based on polymers, metal-metal, ceramic-metal and discusses their use and advantages. 3D printing of super soft hydrogels tends to be very difficult, which is why Dine et al. [7] integrated its own subsystem consisting of a heated dual head into a conventional 3D printer. With the management of the electronics and control of the device, the possibility of precise flow control was achieved even with sharp changes in the speed and direction of printing. Due to the need to print airtight soft products for application in soft robotics and pneumatics, according to Conrad et al. [5] designed printhead replacement device. This tool changer allows you to print flexible products large for pneumatic applications with great precision.

Another possible approach of a changeable tool on a 3D printer is described by Durna et al. [8], who developed a device that, in addition to printing a polymer string, also engraves and divides materials using a laser diode. One more technical solution for a 3D printer with two printheads was proposed by Noorani et al. [15]. The goal was to create a cheap, accurate and fast printer that would surpass the currently used model of a commercial printer.

Currently, there are several commercially available devices which enable multi-colour 3D printing, e. g. Prusa Multi-Material Upgrade 2.0 and tool changer from Prusa Research a.s., or Pallete 2S from Mosaic. Nonetheless, both products allow colour printing with a single material but not printing with multiple materials with different process conditions [22] [23] [24].

Thus, this research aims to propose a constructional solution of a device enabling printing using two different materials, e. g. thermoplastic polyurethane and polyethylene terephthalate glycol. Another important aspect of this work is to ensure that this device can be deployed on an existing Prusa i3MK2S printer. And last but not the least, it is important to maintain the largest possible printing area of the original device.

2 Experimental part

At the beginning of this study, the design and the model of the dual head 3D printer upgrade was prepared. After that, the machine for the 3D printing itself was chosen and finally, the material and suitable process parameters for the print were picked.

2.1 Design solution

The design solution was intended as an upgrade for a commonly available Prusa i3MK2S printer. The upgrade to the printer rests in replacing the old x-axis subassembly for a new one. In our case, this was done by replacing a direct drive extruder by parking extruders, which will be described below.

The main reason for this choice was the ability to print one product from two materials with different extrusion temperatures without having to build a cleaning tower. Another advantage was the compact installation dimensions.

The resulting prototype was composed of purchased and manufactured parts. The construction consisted of two hardened bars that acted as linear guides. As can be seen in Fig. 1, three carriers are movably mounted on the rods (1) using linear ball bearings. The two outer carriages (2) contain extruders and the middle one (3) is equipped with an induction probe measuring the distance from the printing surface. The probe cart is also provided with two solenoids to connect it to the extruder base. The entire movement of the carriages along the linear guide is mediated by a toothed belt (4) which is tensioned between two pulleys (5) located at the ends of the axis. The left pulley is driven by a stepper motor. This moves the toothed belt which is connected to the probe cart. During printing, the probe basement is connected to one extruder carriage using an electromagnet, while the other extruder base is parked at the end of the axis.

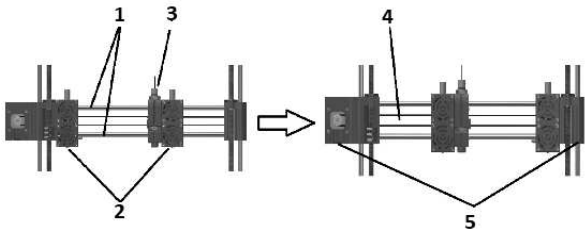

Fig. 1 *Principle of parking extruder function*

The description of the second important assembly is provided in Fig. 2. The filament feeder consists of two stepper motors (1) whose shafts are seated with grooved wheels (2). The ball bearing (3) is always

pressed against the grooved wheels. The filament passes between the bearing and the splined wheel into a bowden (4), which connects the feed device to the extruder. The filament feeder is designed to fit on the top of the Prusa i3MK2S printer, but it can also be screwed anywhere outside the printer.

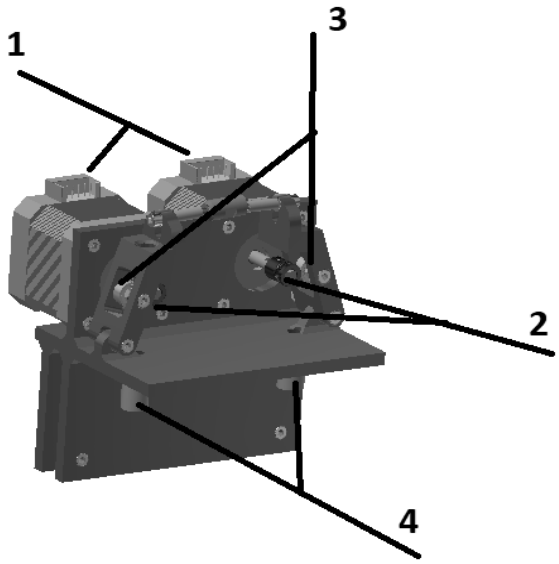

Fig. 2 *Filament Feeder*

2.2 Modelling

Before the modelling itself, a sketch was made on paper providing a rough outline of the overall design and functional parts. Based on this template, models of individually designed parts were created in Autodesk Inventor Professional 2018 CAD software. The individual components were assembled and supplemented with standard parts from libraries and purchased parts from online manufacturers' catalogues. After completion of the assembly, the project documentation was drawn up.

2.3 Static stress analysis

The design also includes a strength analysis of the two most important and most stressed components, namely the left and right ends of the x-axis. Both parts are located at the ends of the x-axis, they are also placed on the bearings of the y-axis, they are connected by hardened rods, and a toothed belt driven by a stepper motor is stretched between them. It is important that this assembly has as little deformation as possible under load. Both parts, like the others, are printed from PET-G material with 30% infill.

Strength analysis was performed using Autodesk Fusion 360 software where the static stress module was selected. For the accuracy of the analysis, the tensile strength value of the PET-G material from the library was adjusted, because the product is printed with 30% infill. With such percentage filling, according to Srinivasan [21], the measured value of tensile strength for printed PET-G corresponds to 19.12 MPa (Fig. 3). By changing this grade, accurate analysis results can be achieved, corresponding to the actual printed part.

Material	PET Plastic 30% infill
Density	1.541E-06 kg / mm^3
Young's Modulus	2.758 GPa
Poisson's Ratio	0.417
Yield Strength	20 MPa
Ultimate Tensile Strength	19.12 MPa
Thermal Conductivity	3E-04 W / (mm C)
Thermal Expansion Coefficient	7.02E-07 / C
Specific Heat	2287 J / (kg C)

Fig. 3 *Properties of PET-G with 30 % infill*

For the strength analysis of the left end of the x-axis, a pair of loads with a value of 100 N was set, which was placed in the two holes for the x-axis hardened bars (Fig 4).

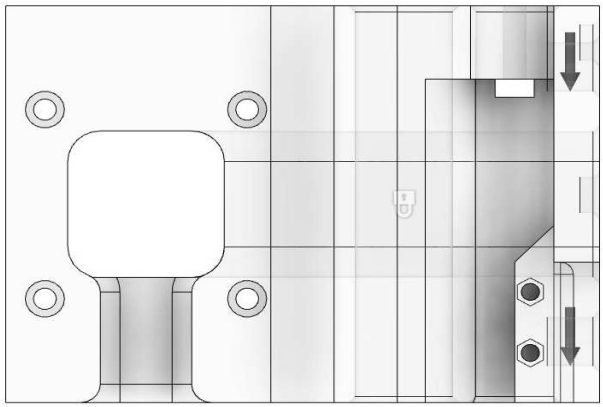

Fig. 4 *Load settings on the left end of axis*

The result of the strength analysis of the left end of the x-axis showed the highest stress achieved at 1.562 MPa, which proved that the part could withstand the given load without any problem. The graphical representation of the results (Fig. 5) is enlarged several times for easy interpretation.

Fig. 5 *Results of stress analysis of the left end of axis*

Another result of this analysis was the displacement of the given part, where the largest displacement value was less than 0.1 mm, namely 0.0133 mm (Fig. 6). This proves that under the given load, the deformation of the part does not affect the accuracy of the entire device in any way. The graphic representation of the displacement is deliberately enlarged for a better interpretation of the results.

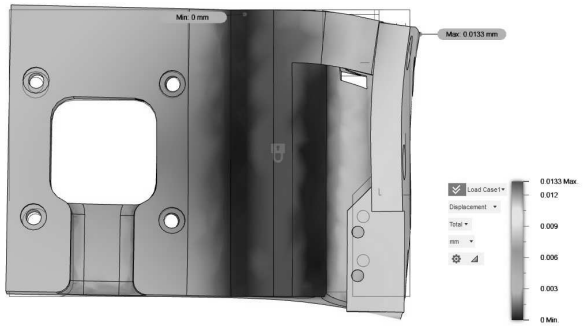

Fig. 6 *Results of the displacement of the left side of axis under stress*

For the strength analysis of the right end of the x-axis, a pair of loads with a value of 100 N was set, which was placed in the two holes for the hardened rods of the x-axis (Fig 7).

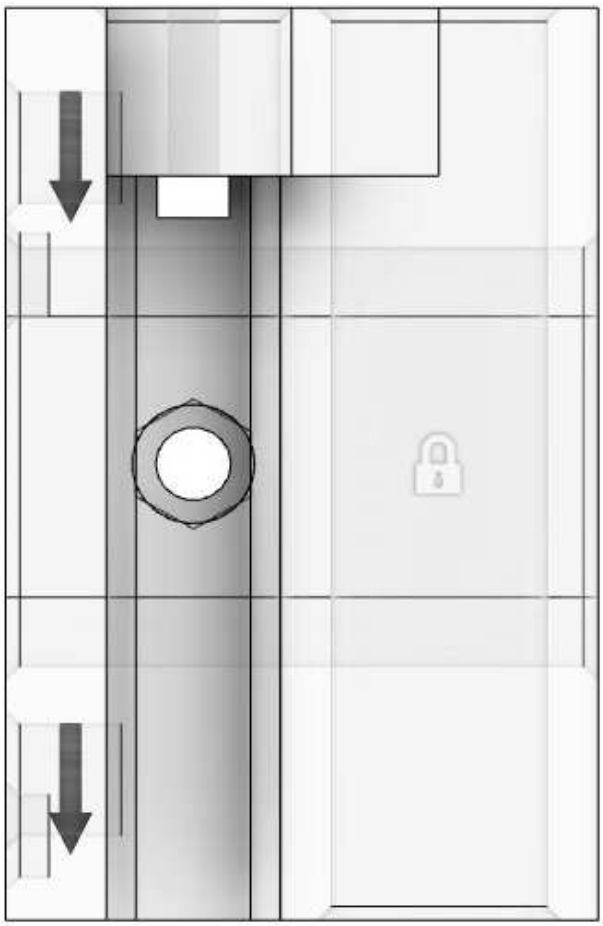

Fig. 7 *Load settings on the right end of axis*

The result of the strength analysis of the right end of the x-axis showed the highest stress achieved at 1.81 MPa, which proved that the part could withstand the given load without any problem. The graphic representation of the results (Fig. 8) is enlarged several times for simple interpretation.

Fig. 8 *Results of stress analysis of the right end of axis*

Another result of this analysis was the displacement of the given part, where the largest displacement value was less than 0.1 mm, specifically 0.0145 mm (Fig. 9). This proves that under the given load, the deformation of the part does not affect the accuracy of the entire device in any way. The graphic representation of the displacement is deliberately enlarged for a better interpretation of the results.

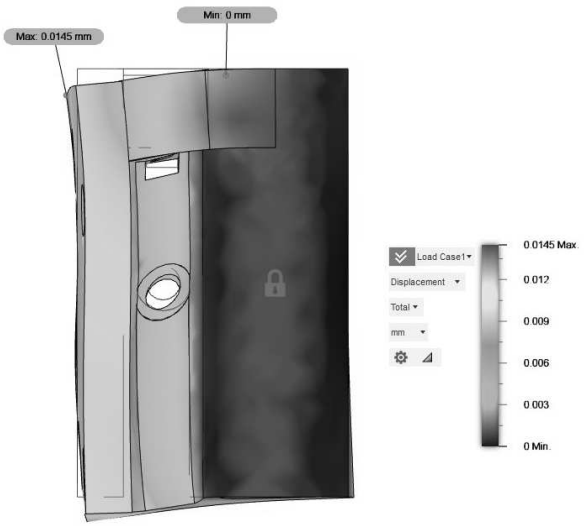

Fig. 9 *Results of the displacement of the right side of axis under stress*

2.4 Slicer

To create 3D models, student licensed Autodesk Inventor Professional 2018 CAD software was used.

Further, Prusa Slic3R software was used to create the G-code by inserting the prepared models and pressing the button "generate" (Fig. 10).

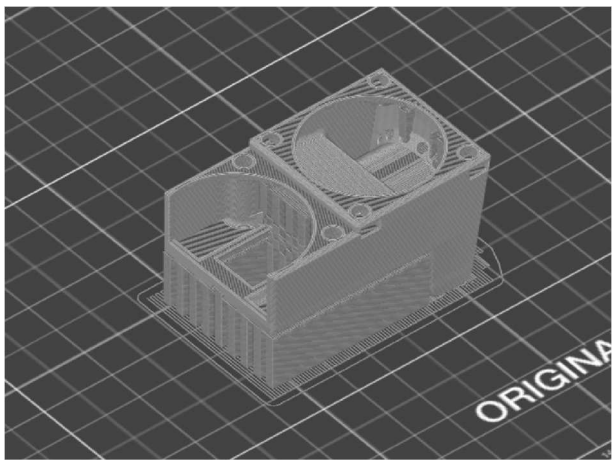

Fig. 10 *3D model sliced in Prusa Slic3r*

2.5 Materials

For component printing PET-G was chosen, due to its good mechanical properties. This material excels in providing good mechanical properties and smooth printing process. The trade name of the material is PET-G - Transparent Green, from the Polish manufacturer Devil Design. The manufacturer's recommended heat bed temperature is 70 - 80 °C and the nozzle temperature is 220 – 250°C.

2.6 Process settings

When selecting process conditions in the Prusa Slic3r software, an infill density was set at 30% and a layer height of 0.15 mm was selected (Fig. 11). The printing temperature was set to 245 °C on the extruder and 80 °C on the heat bed. The printing speed was set to 60 mm/s.

Fig. 11 *Process settings from Slic3r Prusa Edition software*

3 Results

The main result of this work was the assembly of an upgrade for the Prusa i3MK2S printer which enables the printing of products from two different materials. After printing individual parts, a prototype was assembled with both purchased and manufactured parts. In the following, the parts created with the process parameters, printer, and material will be described. Then, all the parts will be shown within the assembly.

3.1 Extruder carriers

The extruder carriers (Fig. 5) are mirror-symmetrical components which are made in two pieces. The extruder holds in place as it is tightened by screws between the cover and the extruder carriage. At the rear, it has two holes for pressing bearings (1). On the upper side, there is a through-hole, partially provided with a thread for holding a straight fitting through which the filament passes into the extruder (2). On the one side, it is always provided with a pocket for screwing on the contact of the electromagnet (3), and the other side with two smaller pockets (4) for accommodating neodymium magnets serving for anchoring in the correct position. On the same side where the contact of the magnet is located, there is also a pocket for screwing the guide pin (5) in the lower part. The extruder cover (6) is also screwed to the extruder carriage with four M3 screws. Hexagon nuts are used to tighten these screws, which are inserted into rectangular pockets that are on both sides of the extruder carriage (7).

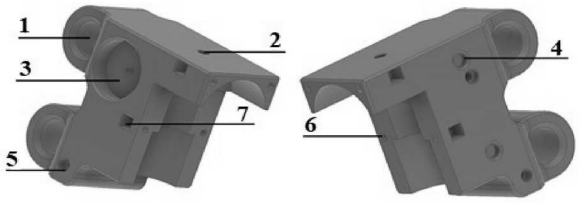

Fig. 12 *Extruder carrier from the left and the right side*

3.2 Extruder cover

The extruder cover (Fig. 13) is a very complex component for attaching the extruder to the extruder carriage (1). Furthermore, air distribution is made in it both for cooling the extruder and for cooling the printout itself. Two inlet openings (3) are used to supply air from the fans. The entire extruder cover is bolted with six M3 screws, both to the extruder carriage and to the fan cover (4). The hexagon nuts that tighten the fan cover are housed in rectangular pockets on the sides of the extruder cover (5). The extruder cover is printed in two pieces - each for one extruder carriage.

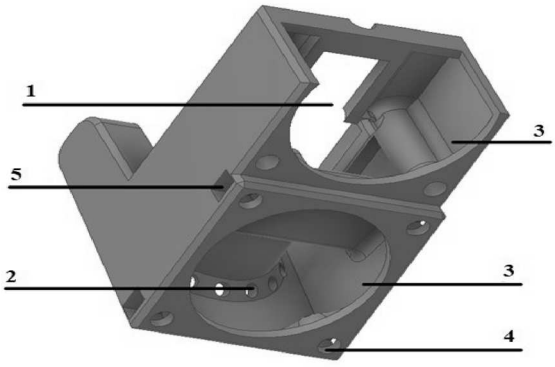

Fig. 13 *Extruder cover*

3.3 Fan mounts

The fan holder (Fig. 14) is used to screw the fans to the extruder carriage and the extruder cover. The upper fan is used to cool the extruder and nozzle, while the lower one is used to cool the just extruded filament. The fan holder has eight holes for M3 screws. Two pieces are made - one for each extruder carriage.

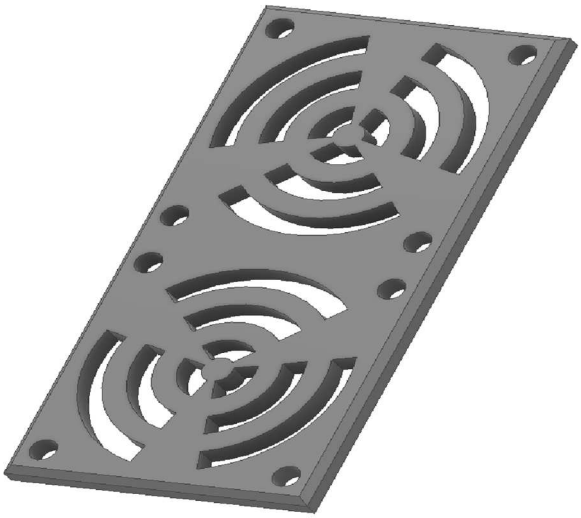

Fig. 14 *Fan mount*

3.4 Probe carrier

The probe carrier (Fig. 15) has two holes for pressing bearings (1). Between them is the space for the tooth belt clutch (2). On the left and the right sides, there are pockets for screwing on electromagnets (3). The through-hole serves to insert the guide pin (4). There are two holes on the top. The smaller one is used to lead the electrical cables from the electromagnets (5), while the larger one is determined to route the induction probe (6). Furthermore, two holes (7) are led through the probe carriage for M3 size screws which are to help fix the induction probe. The pocket created through the hole for the induction probe is used to tighten the fixing nut size M12 (8).

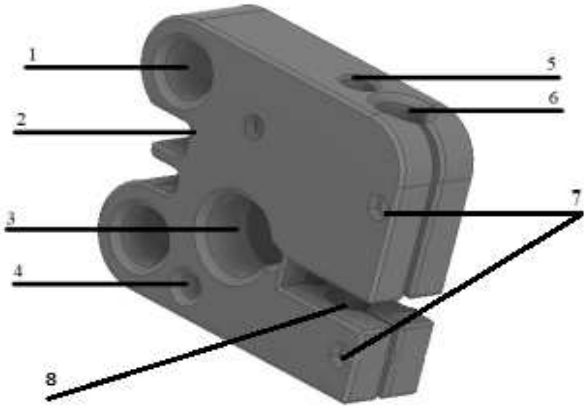

Fig. 15 *Probe carrier*

3.5 Left/right end of x-axis

The left end of the x-axis (Fig.16) together with the right end fix the linear guide, a toothed belt is stretched between them to move the probe carriage. The left and right ends of the x-axis also function as housings for the bearings (1), a trapezoidal nut (2) allowing the entire assembly to move in the z-axis. It is anchored in place by four M3 screws (3). There is also a limit switch on the left side, which is fastened with M2 screws (4). Both ends of the x-axis also have an opening (5) through which the toothed belt guides. Furthermore, on the inner sides of both ends there are also holes (6) into which neodymium magnets are pressed, holding the parked extruder in place.

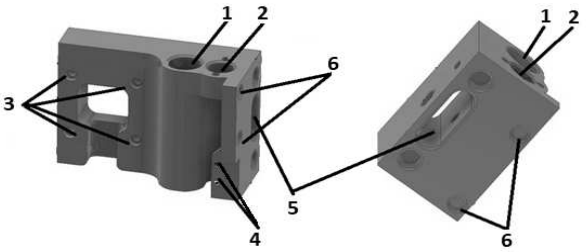

Fig. 16 *The left and the right end of x-axis*

3.6 Filament holder

Filament feeder holder (Fig. 17) designed for mounting on the top frame of the printer, or anywhere outside the printer. For mounting on the upper frame, a cut-out is created, in the lower part of which two holes are made for M3x16 screws, at the rear with shoulders for hexagon nuts (1). The upper part contains fittings for two stepper motors, each of which is attached with four M3x10 screws (2). In the places below the shafts coming out of the stepper motors, the through-hole is provided with a thread into which a straight fitting connection is screwed, through which the filament (3) passes. On the left and right side, the protrusions are provided with radii and holes in their axes, through which are guided M3x20 screws holding the pulley holders in place (4).

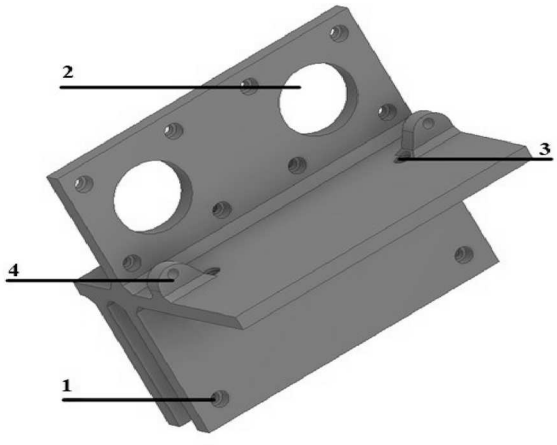

Fig. 17 *Feeder holder*

3.7 Pulley holder

The pulley holder (Fig. 18) is screwed to the filament drive holder with an M3x20 screw (1). A pulley consisting of one bearing 623 2Z, three hexagon nuts M3 and a screw M3x20 (fits in the holes 2 and 3), which performs the function of the shaft.is attached to it. The second function of the pulley holder is to tension it against the grooved wheel of the filament feeder using the M3x25 screw (4). An opening pass through the pulley holder through which the filament passes into the feeder (5). The whole part is printed in two pieces - one for each pulley.

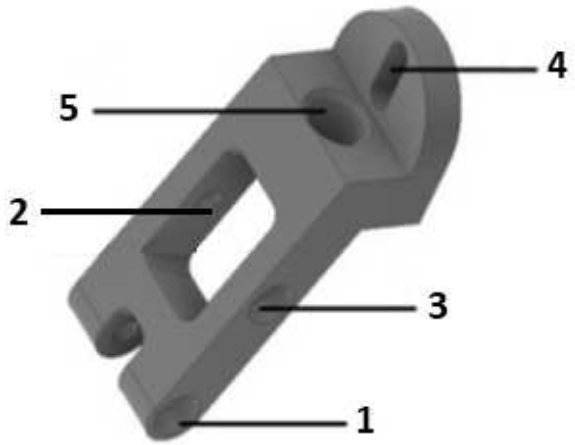

Fig. 18 *Pulley holder*

3.8 Tooth belt clutch

Tooth belt clutch (Fig. 19) ensuring the connection and tensioning of the toothed belt. The clutch is located on the back of the probe carrier.

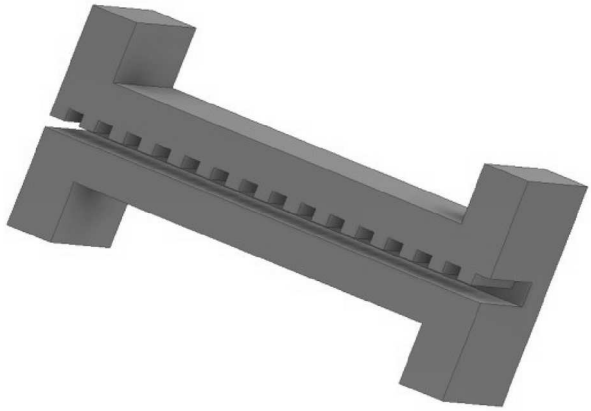

Fig. 19 *Tooth belt clutch*

3.9 Assembly

Fig. 20 provides an overview of where each part was created fits. In our research, every single part fitted perfectly in its prepared slot due to the precise dimensions of 3D printing.

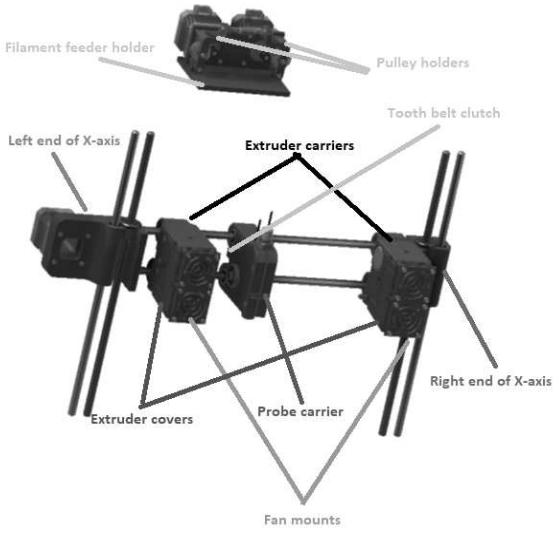

Fig. 20 *Printed parts in the assembly*

Finally, Fig. 21 shows the real assembly which was photographed after the individual pieces were put together.

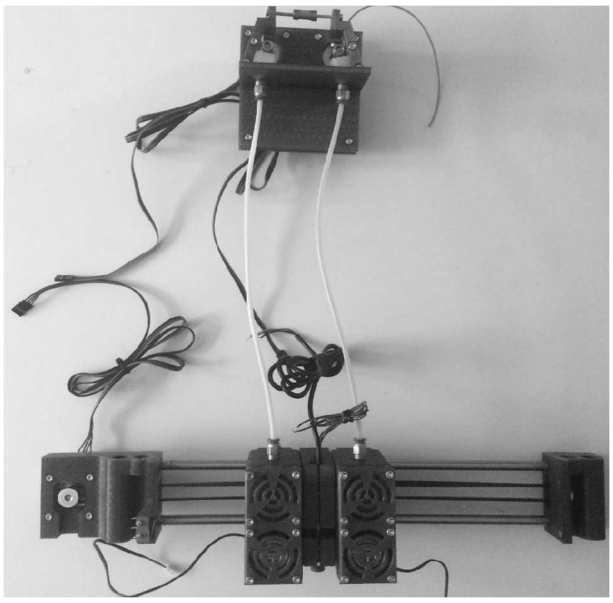

Fig. 21 *Assembled prototype*

4 Discussion

This assembled prototype can be fitted on the selected 3D printer, which satisfies the goal set at the beginning of this paper. The overall size of the printing area was reduced only minimally, which was another appointed goal. The most stressed parts of the assembly, the left and right ends of the axis, were subjected to static stress analysis using the Autodesk Fusion 360 program, where the results showed that the maximum stress was not exceeded anywhere, and the total deformation does not affect the accuracy of the entire device. The testing of the prototype on the printer itself was not performed during this research, because it is necessary to modify the printer firmware,

which will be part of the following research which also includes a solution for easy calibration of both nozzles. Main advantage of this solution is the possibility to easily re-design for another 3D printer with a Cartesian frame. In this case, it is only a matter of changing the length of the guide rods, or the diameters of the holes for the bearings.

5 Conclusions

The primary aim of this work was to create a design which could be manufactured into a prototype of a device enabling dual extrusion/printing. The entire design focused on the design of an x-axis assembly, which works on the principle of parking extruders with an external drive of the filament transported in the bowdens. The entire x-axis assembly was designed to be compatible with the Prusa i3MK2S printer, which was also used to print the designed parts. Before printing, the most stressed parts of the assembly were checked using an analysis in the Autodesk Fusion 360 software. The result of this analysis was that both parts resisted the applied stress, and the resulting deformation will not affect the accuracy of the entire assembly in any way. These printed components, along with the purchased parts, were assembled into a prototype assembly. Due to this step, the compatibility with the Prusa i3MK2S printer and minimal reduction in printing space could be verified. One of the biggest advantages of this device is its simplicity. It is quite easy to replace the linear guide with a guide of different length, whereby selectable dimensions of the printing surface can be obtained. By creating a tangible prototype of this device and obtaining results that meet the specifications, the development of an available printer that allows multi-material printing can continue. The following research will set its focus on the development of an entirely new printer, instead of just an addition to an already existing one. The reason for this choice rests in greater freedom to install upgrades and better availability of this type of printer in the market.

Acknowledgement

This work was supported by the Internal Grant Agency of TBU in Zlin: no. IGA/FT/2023/005.

References

[1] ALI, M.H. AND MIR-NASIRI, N. (2015) "Multi-nozzle extrusion system for 3D printer and its control mechanism," *The International Journal of Advanced Manufacturing Technology*, 86(1-4), pp. 999–1010. Available at: https://doi.org/10.1007/s00170-015-8205-9

[2] BANDYOPADHYAY, A. AND HEER, B. (2018) "Additive manufacturing of multi-material structures," *Materials Science and Engineering: R: Reports*, 129, pp. 1–16. Available at: https://doi.org/10.1016/j.mser.2018.04.001

[3] BLOK, L.G. AND LONGANA, M.L. (2018) "An investigation into 3D printing of Fibre Reinforced Thermoplastic Composites," *Additive Manufacturing*, 22, pp. 176–186. Available at: https://doi.org/10.1016/j.addma.2018.04.039

[4] CHEN, Y. AND SHI, T. (2019) "Optimization design of color mixing nozzle based on multi physical field coupling," *IOP Conference Series: Earth and Environmental Science*, 233, p. 032004. Available at: https://doi.org/10.1088/1755-1315/233/3/032004

[5] CONRAD, S. AND SPECK, T. (2021) "Tool changing 3D printer for rapid prototyping of advanced soft robotic elements," *Bioinspiration & Biomimetics*, 16(5), p. 055010. Available at: https://doi.org/10.1088/1748-3190/ac095a

[6] SANCHEZ DE LA NAVA, A.M. AND LIBEROS, A. (2017) "Dual extruder 3D-bioprinter for computer designed cardiac structures," *Computing in Cardiology Conference (CinC)* [Preprint]. Available at: https://doi.org/10.22489/cinc.2017.146-273

[7] DINE, A. AND BENTLEY, E. (2021) "A dual nozzle 3D printing system for Super Soft Composite hydrogels," *HardwareX*, 9. Available at: https://doi.org/10.1016/j.ohx.2021.e00176

[8] DURNA, A. AND FRIES, J. (2020) "Research and development of laser engraving and material cutting machine from 3D printer," *Management Systems in Production Engineering*, 28(1), pp. 47–52. Available at: https://doi.org/10.2478/mspe-2020-0008

[9] HAN, S. AND XIAO, Y. (2017) "Design and analysis of fused deposition modeling 3D printer nozzle for color mixing," *Advances in Materials Science and Engineering*, 2017, pp. 1–12. Available at: https://doi.org/10.1155/2017/2095137

[10] JAKSA, L. AND PAHR, D. (2021) "Development of a multi-material 3D printer for functional anatomic models," *International Journal of Bioprinting*, 7(4), p. 420. Available at: https://doi.org/10.18063/ijb.v7i4.420

[11] KOCH, F. AND THADEN, O. (2021) "Open-source hybrid 3D-bioprinter for simultaneous printing of thermoplastics and Hydrogels,"

HardwareX, 10. Available at: https://doi.org/10.1016/j.ohx.2021.e00230

[12] KUN, K. (2016) "Reconstruction and development of a 3D printer using FDM Technology," *Procedia Engineering*, 149, pp. 203–211. Available at: https://doi.org/10.1016/j.proeng.2016.06.657

[13] LAURETO, J. AND PEARCE, J. (2017) "Open-source multi-head 3D printer for polymer-metal composite component manufacturing," *Technologies*, 5(2), p. 36. Available at: https://doi.org/10.3390/technologies5020036

[14] LIIMATAINEN, K. AND LATONEN, L. (2019) "3D-printed whole prostate models with tumor hotspots using dual-extruder printer," *2019 41st Annual International Conference of the IEEE Engineering in Medicine and Biology Society (EMBC)* [Preprint]. Available at: https://doi.org/10.1109/embc.2019.8857068

[15] NOORANI, R. AND LYNCH, M. (2019) "Design and manufacturing of a 3D printer for teaching and research," *IOP Conference Series: Materials Science and Engineering*, 652(1), p. 012058. Available at: https://doi.org/10.1088/1757-899x/652/1/012058

[16] OTEPBERGENOV, T. AND SMAGULOV, Z. (2020) "Numerical and experimental analysis of the 3D printed multi-material ankle-foot orthosis," *Journal of Physics: Conference Series*, 1510(1), p. 012012. Available at: https://doi.org/10.1088/1742-6596/1510/1/012012

[17] REINER, T. AND CARR, N. (2014) "Dual-color mixing for fused deposition modeling printers," *Computer Graphics Forum*, 33(2), pp. 479–486. Available at: https://doi.org/10.1111/cgf.12319

[18] ROACH, D.J. AND HAMEL, C.M. (2019) "The M4 3D printer: A multi-material multi-method additive manufacturing platform for future 3D printed structures," *Additive Manufacturing*, 29, p. 100819. Available at: https://doi.org/10.1016/j.addma.2019.100819

[19] SITTHI-AMORN, P. AND RAMOS, J.E. (2015) "Multifab," *ACM Transactions on Graphics*, 34(4), pp. 1–11. Available at: https://doi.org/10.1145/2766962

[20] SODUPE-ORTEGA, E. AND SANZ-GARCIA, A. (2018) "Accurate calibration in multi-material 3D bioprinting for tissue engineering," *Materials*, 11(8), p. 1402. Available at: https://doi.org/10.3390/ma11081402

[21] SRINIVASAN, R. AND RUBAN, W. (2020) "Effect on infill density on mechanical properties of PETG part fabricated by fused deposition modelling," *Materials Today: Proceedings*, 27, pp. 1838–1842. Available at: https://doi.org/10.1016/j.matpr.2020.03.797

[22] ISSAYEV, G. AND HAZRAT ALI, MD. (2021) "Bonding Strength Analysis of Multi-material and Multi-color Specimens Printed with Multi-extrusion Printer" *Manufacturing technology*, 21(5), pp. 627–633. Available at: https://doi.10.21062/mft.2021.072

[23] PIS, D. AND HANUSOVA, K. (2022) "Degradation of 3D Printed Polymer Composites with Filler of Cellulose-Based Materials" *Manufacturing technology*, 22(3), pp. 327–333. Available at: https://doi.10.21062/mft.2022.041

[24] SEDLAK, J. AND HORAK, O. (2022) "Determination of Mechanical Properties of Plastic Components Made by 3D Printing" *Manufacturing technology*, 22(6), pp. 733–746. Available at: https://doi.10.21062/mft.2022.082